Research Article

Differential Bearing Estimation for RF Tags

Ákos Lédeczi, János Sallai, Péter Völgyesi, and Ryan Thibodeaux

Institute for Software Integrated Systems, Vanderbilt University, Nashville, TN 37235, USA

Correspondence should be addressed to Ákos Lédeczi, akos.ledeczi@vanderbilt.edu

Fusing spatially distributed observations in wireless sensor networks or asset tracking in a shipyard are just two-example applications where the location of radio nodes needs to be known. Localization and tracking of wireless nodes have been an active research area, yet a universal solution has not emerged so far. This paper introduces a novel method for bearing estimation based on a rotating antenna generating a Doppler shifted RF signal. The small frequency change can be measured even on low-cost resource constrained nodes using a radio interferometric technique introduced previously. Bearing information between anchors nodes at known locations and RF tags at unknown positions can be derived. A few such measurements provide enough information to enable accurate node localization.

1. Introduction

While there are many practical localization systems for mobile ad hoc networks, wireless sensor networks (WSN) and unattended air or ground vehicles (UAV, UGV), there are still applications with such requirements that none of the existing solutions is satisfactory. GPS, for example, typically does not work indoors and it is also not well suited when low cost and/or very long lifetime are the main design drivers. Techniques based on ultrasonic and infrared signal modalities have short range and require line-of-sight. Clearly, RF-based approaches have many advantages for most applications. A radio is already available on any wireless node, so it comes at no added cost and it is already included in the power budget. RF range is superior to most other signals. Line-of-sight may not be necessary, since radio signals may propagate through walls; however, radio propagation, especially indoors, presents significant problems of its own.

Radio signal strength (RSS)-based approaches are the most straightforward for estimating distance from an RF signal; however, such methodologies are relatively imprecise due to fading. The accuracy of numerous RSS techniques is typically meter-scale [1–3]. A few commercial systems, such as PinPoint [4], based on time of arrival (TOA) and RSS measurements have also been developed with similar accuracy. The Location Engine [5] developed at Motorola Research depends on RSS measurements and anchor nodes at known positions. Chipcon (now Texas Instruments) licensed and integrated the technology into the CC2431 transceiver chip and claims 3 m accuracy.

Active RFID systems use self-powered tags to identify and locate objects. LANDMARC relies on multiple-fixed RFID readers and reference tags. It estimates the proximity of a given tag to reference tags by correlating their respective signals by multiple readers [6]. The accuracy achieved is meter-scale with high enough reference tag density. PanGo is a commercial asset tracking system using 802.11 active RFID tags [7] providing room-level resolution relying on dense access point infrastructure.

Ultra-Wideband (UWB) systems are resistant to multipath effects in both communication and ranging. UWB-based range measurements have accuracy of 1.5 m or better [8, 9]. Ubisense has recently developed a UWB-based fine-grained localization system with an accuracy of about 20 cm [10]. The disadvantage of UWB is that it relies on the time-of-flight of radio signals; hence, it requires high sampling rates and/or nanosecond-scale time synchronization thus increasing cost. Also, the Federal Communications Commission (FCC) has limited the maximum power of UWB radio transmissions restricting the maximum range of UWB methods typically to 20 m [11, 12].

Recently, a radio interferometric solution was proposed for the localization and tracking of resource-constrained wireless nodes [12–15]. By measuring the phase difference of a signal generated by two transmitters with close frequencies at two receivers, information on the relative distances of the four nodes involved can be deduced. In addition to the node transmitting a sinusoid of frequency f, an auxiliary node is transmitting a sinusoid of frequency $f - f_i$. The superposition of the two signals generates an interference field with beat frequency f_i. Tuning the transmitters, so that the interference frequency f_i is a few hundred Hz, makes it possible to measure the phase of the signal with resource-constrained wireless nodes. The receiver can observe the low-frequency beating using the the received signal strength indicator (RSSI) signal provided by the RF transceiver chip. The RSSI signal is the power of the incoming signal mixed down to an intermediate frequency and low-pass filtered. It was shown in [12] that a phase change in the high-frequency sinusoid results in an equivalent phase change in the RSSI signal. Taking the difference of the phases observed at two receivers eliminates the unknown initial phases of the transmitters. However, it complicates the ranging because one measurement provides information on the pairwise distances of four nodes, but making multiple measurements in a network of at least six nodes provides enough information to compute the relative location of all nodes.

While both the range and the accuracy of the method proved superior to many other approaches [3, 16, 17] in open areas, multipath propagation impacts the accuracy of the technique. A variation of the method replaces the phase measurements with that of frequency. The technique assumes a moving transmitter at an unknown location (and with an unknown velocity vector). As such, it generates a Doppler shift. The reference implementation works on Crossbow Mica2 nodes operating at 430 MHz [18]. A person walking with the transmitter at 0.3 m/s induces a 0.4 Hz shift, a $10^9 : 1$ ratio, which is impossible to measure on the cc1000 radio chip or on much more expensive instrumentation either. However, the radio interferometric approach works here as well; the same amount of Doppler shift appears in the beat signal as in the carrier [15] and it can be measured accurately enough using simple, inexpensive hardware. If this shift is measured at multiple receivers, the location and velocity of the tag can be accurately estimated [19].

The obvious disadvantage of this method is the requirement for movement, since without it, there would be no Doppler shift. This observation led us to the idea of rotating the antenna of the transmitter (or even the entire node) at a constant speed and radius. To a stationery observer, the signal will have a continuously changing frequency due to the Doppler effect. Again, radio interferometry is required to be able to measure this accurately. How the frequency changes over time depends on the angular velocity of the transmitter, the radius of the circle, and the distance between the rotating transmitter and the receiver. While it is trivial to compute the distance given the radius and the angular velocity, the result is very sensitive to measurement errors if the distance is large. To tackle this issue, we leverage the fact that the correlation

of the observed frequency change across multiple receivers provides valuable information on the location of the nodes involved. In this paper, we analyze the case of localizing a rotating transmitter using fixed receivers at known locations.

The remainder of the paper is structured as follows. In Section 2, we develop a differential bearing estimation approach which is based on Doppler frequency measurements. The signal processing technique to estimate the Doppler-shifted frequency is described in Section 3. Then, in Section 4, we propose a localization algorithm based on differential bearing estimates. We present experimental and simulation results in Section 5 and conclude the paper assessing the practical applicability of our technique and highlighting future research directions.

2. Ranging Approaches

Rotating a radio transmitter results in a continuously changing frequency at a stationary observer due to the Doppler effect. The frequency f_R observed by receiver R depends on the relative speed v of the transmitter with respect to the observer (negative if they move away from each other, positive if they move toward each other):

$$f_R = f_T \frac{c}{c - v}, \tag{1}$$

where f_T is the baseline frequency emitted by the transmitter and c is the speed of light.

Since the speed of light is much larger than the velocity of the transmitter, the above formula can be written as

$$
\begin{aligned}
f_R &= f_T \left(1 + \frac{v}{c - v} \right) \\
&\approx f_T \left(1 + \frac{v}{c} \right) \\
&= f_T + \frac{f_T v}{c} \\
&= f_T + \frac{v}{\lambda},
\end{aligned}
\tag{2}
$$

where $\lambda = f_T/c$ is the wavelength of the transmitted signal. That is, the doppler shift is

$$f_R - f_T \approx \frac{v}{\lambda}. \tag{3}$$

When using radio-interferometry as described in Section 1, that is, a stationary auxiliary transmitter is emitting a sine wave of frequency $f_T - \epsilon$ (where $\epsilon \ll f_T$), it was shown in [15] that the same amount of Doppler shift appears in the low-frequency envelope signal.

Consider Figure 1 where transmitter T rotates at a constant angular rate ω and radius r and receiver R measures the frequency of the signal. The maximum of the frequency is observed at point A where the transmitter moves directly toward the receiver, while the minimum frequency is measured when the transmitter is at point B moving exactly away from the receiver. By measuring the time Δt between the two extrema of the frequency shift, the angle β can be estimated given the angular speed of the transmitter.
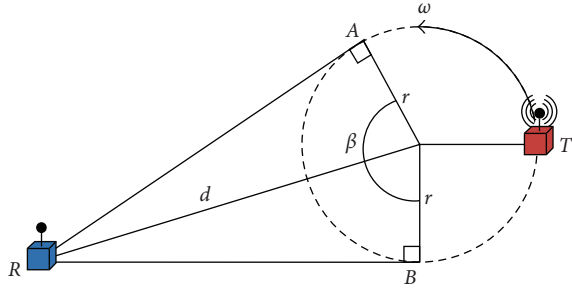
FIGURE 1: Range estimation method.

The distance d between the receiver and the center of rotation of the transmitter is then

$$d = \frac{r}{\cos(\beta/2)} = \frac{r}{\cos(\omega \Delta t/2)}. \tag{4}$$

Hence, the range between two nodes can be estimated this way.

One of the advantages of the above ranging method is that one does not need the actual magnitude of the frequency shift, only the time of the maximum and minimum frequency values. Figure 2(a) shows the expected Doppler shift observed by the receiver when it is 10 meters away from the rotating transmitter. Unfortunately, any measurement has error. The question is how it affects the accuracy of ranging? Consider (4) again. Reformulating the equation, one can plot the expected value of the measured angle as a function of the distance between the receiver and the center of rotation of the transmitter. Figure 2(b) shows this function with a corresponding rotation radius of 12 cm. One can see that the function gets flat fast. For example, the angle difference between 20 and 21 meters is about 0.03 degrees. That is clearly beyond the expected accuracy of this measurement. In fact, the ranging error beyond only 5 meters would be unacceptably high.

However, introducing a second receiver offers another method for ranging. Consider Figure 3. Both receivers R_1 and R_2 continuously measure the frequency of the signal. Let $\vec{v}(t)$ denote the velocity vector of the rotating transmitter at time t. Let us define $v_1(t)$ and $v_2(t)$ as the (signed) speed of the rotating transmitter with respect to stationary receivers R_1 and R_2 at time t. Formally,

$$v_1(t) = \frac{\vec{v}(t) \cdot \vec{TR_1}}{|\vec{TR_1}|},$$
$$v_2(t) = \frac{\vec{v}(t) \cdot \vec{TR_2}}{|\vec{TR_2}|}. \tag{5}$$

From the velocities at time t_1 when R_1 observes the maximal frequency, we can compute the angle $\alpha = \angle R_1 T R_2$ (the angle at which the segment $R_1 R_2$ can be seen from T) as

$$\alpha = \cos^{-1} \frac{v_2(t_1)}{v_1(t_1)}. \tag{6}$$

Given α, it can be easily shown that R_1, T, and R_2 need to be on a circle with a radius of

$$r_{\text{circle}} = \frac{l}{2\sin(\alpha)}, \tag{7}$$

where l is the distance between receivers R_1 and R_2. While we obtain an angle, the result is still similar to traditional pairwise ranging in that one "range" estimate constrains the location of the node to a circle. Except the center of the circle in our case is not another node, but a location that can be computed from the locations of the two receivers and the measured angle.

While attractive, this method relies on measuring the Doppler shift at any one receiver accurately. However, in most computers and wireless devices, uncompensated crystal oscillators are used to generate the clock signals. The short-term stability of these oscillators are typically between 10^{-8} and 10^{-9} for one second. In our case, this corresponds to possibly more than 1 Hz error that cannot be compensated for, because we cannot measure the baseline frequency directly (i.e., when the transmitter is stationary). We need to rely on measuring the difference between the maximum and the minimum frequencies and take their mean. Since the time between these events may not be much less than one second, short term stability can cause a larger error than the phenomenon we are trying to measure. Temperature-compensated crystal oscillators have somewhat better stability, while oven-controlled crystal oscillators are at least an order of magnitude more precise. Unfortunately, their price and power requirements are both significantly higher, and they are not used in everyday devices. The question is then how can we eliminate this significant source of error?

Note that it is only the transmitter instability that is important here, because the radio interferometric technique already eliminates the receiver instability by using the envelope signal. Notice that the transmit frequency instability has the same effect at both receivers because we compare their measurements at the same time. Hence, if we take the difference of the two measured frequencies, the actual transmit frequency is eliminated. This frequency difference relates to the difference of the observed speeds; however, not having the speed measurements available individually, only their difference, makes solving for the location somewhat more complicated. Let $\Delta f(t)$ denote the difference of the observed frequencies f_{R_1} and f_{R_2} for receivers R_1 and R_2 at time t. If we assume that $c \gg v_1(t)$ and $c \gg v_2(t)$, we can write the measured frequency difference using (2) as

$$\begin{aligned} \Delta f(t) &= f_{R_1}(t) - f_{R_2}(t) \\ &\approx \frac{f_T}{c}(v_1(t) - v_2(t)) \\ &= \frac{v_1(t) - v_2(t)}{\lambda}, \end{aligned} \tag{8}$$

and we now write

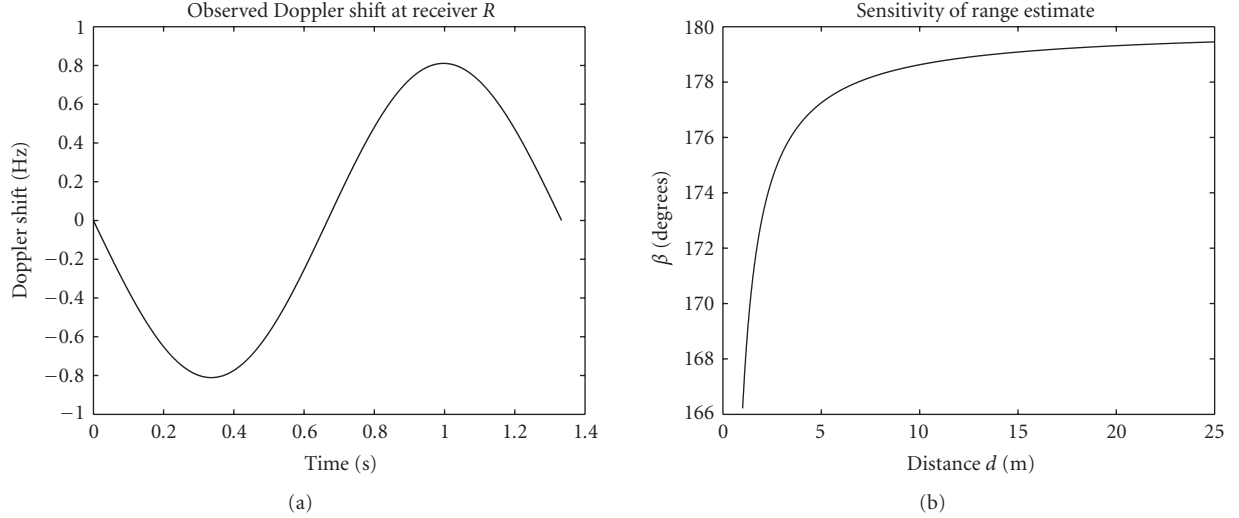$$\Delta v(t) = v_1(t) - v_2(t). \tag{9}$$

(a)

(b)

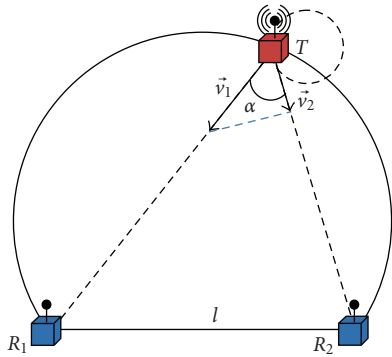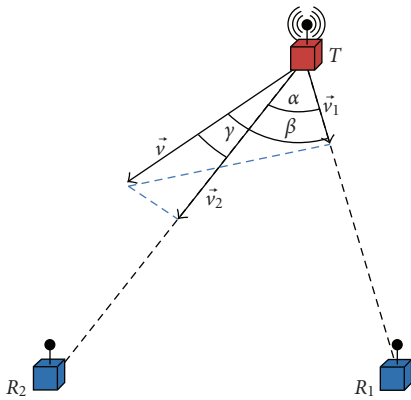FIGURE 2: Range estimation results.

FIGURE 3: Range estimation from α angles.

FIGURE 4: Computation of angles.

Let us define angles $\beta(t)$ and $\gamma(t)$ as the angle between the velocity vector $\vec{v}(t)$ of transmitter T and its components pointing toward receivers R_1 and R_2, respectively. From Figure 4 we see that (5) can be rewritten as $v_1(t) = |\vec{v}(t)| \cos(\beta(t))$ and $v_2(t) = |\vec{v}(t)| \cos(\gamma(t))$.

To simplify further computation, we assume that the receivers are far from the circle of rotation, that is, $TR_1 \gg r$ and $TR_2 \gg r$. If the radius of the circle is small compared to the distance between the transmitter and the receiver, the error this assumption introduces is minimal. With this so called *far field* assumption, the angle $\angle R_1 T R_2$, denoted as α, is fixed. Without the loss of generality, let us assume that $\beta(0) = 0$. Therefore, $\beta(t) = \omega t$ and $\gamma(t) = \beta(t) - \alpha$. Substituting these relationships into (9) yields

$$\Delta v(t) = |\vec{v}(t)| (\cos(\omega t) - \cos(\omega t - \alpha)). \quad (10)$$

Using the trigonometric identity for the difference of cosines

$$\cos\theta - \cos\varphi = -2\sin\left(\frac{\theta + \varphi}{2}\right)\sin\left(\frac{\theta - \varphi}{2}\right), \quad (11)$$

we can rewrite (10) as

$$\Delta v(t) = -2|\vec{v}(t)| \sin\left(\frac{2\omega t - \alpha}{2}\right)\sin\left(\frac{\alpha}{2}\right), \quad (12)$$

$\Delta v(t)$ takes its maximum, where the first sine equals -1:

$$\max(\Delta v(t)) = 2|\vec{v}(t)| \sin\left(\frac{\alpha}{2}\right). \quad (13)$$

From here, using (8), α can be expressed as follows:

$$\alpha = 2\sin^{-1}\left(\frac{\max(\Delta v(t))}{2|\vec{v}(t)|}\right) = 2\sin^{-1}\left(\frac{\max(\Delta f(t))}{2\lambda|\vec{v}(t)|}\right). \quad (14)$$

Therefore, by measuring the maximum difference of the Doppler shifts measured at receivers R_1 and R_2, we can estimate α. In the presence of noise, however, the maximum of the signal cannot be measured precisely. Obviously,

measurement noise can be mitigated by iteratively measuring $\max(\Delta f(t))$ and averaging the observed values, though such a technique is time consuming.

We observe that not only the maximum measured value, but the magnitude of all the measured values are related to α. To make use of this, we can measure the power of the signal instead, because it is more resilient to noise due to the integration. Since the average power of a sine wave is 1/2 times its amplitude, we get that

$$\alpha = 2\sin^{-1}\left(\frac{P_{\mathrm{avg}}(\Delta v(t))}{|\vec{v}(t)|}\right) = 2\sin^{-1}\left(\frac{P_{\mathrm{avg}}(\Delta f(t))}{\lambda |\vec{v}(t)|}\right), \quad (15)$$

where

$$P_{\mathrm{avg}}(\Delta f(t)) = \frac{\omega}{2\pi}\int_0^{2\pi/\omega}\Delta f^2(t)dt. \quad (16)$$

Therefore, it is sufficient for the two receivers to measure the frequency of the received signal for the duration of merely one rotation in order to compute α.

3. Frequency Estimation

We selected the GNU Radio [20] software platform and the USRP [21] hardware frontend to verify the proposed ranging ideas. The Software Defined Radio (SDR) is an ideal tool for experimentation, since it allows for rapid prototyping of experimental algorithms. Using an SDR is a promising approach not only for increasing the computational budget, but also for making detailed observations on the signals. While SDR is a more powerful and more flexible platform than those used previously in radio interferometric localization [12–14], our primary goal was to test and fine-tune the proposed algorithms using an SDR, then to port the final solution to low-power wireless nodes, such as the Berkeley Mica2 or the XSM mote [22].

The baseline configuration consists of a fixed position SDR transmitter and a rotating transmitter. The rotating node emits a pure sine wave continuously, thus it can be implemented using a simple, low-cost device, such as a WSN. The fixed position transmitter transmits a pure sine wave at a close frequency. Since multiple receivers need to make synchronized measurements, a time synchronization approach is necessary. Instead of implementing a time synchronization protocol on the SDR platform, we embed timing information in the transmitted signal itself. The SDR transmitter periodically emits a windowed chirp signal before a pure sine wave segment. That chirp can be accurately decoded on the receiver side and it makes a common time reference point for all receivers. The range of this short frequency sweep does not overlap with the frequencies of the pure sinusoids.

The architecture of a receiver node is shown in Figure 5. The top part of the diagram demonstrates the signal flow in the RF frontend and the USRP digital frontend. The selected RF module can be tuned in the 400–500 MHz range by controlling the onboard PLL. The downconverted and amplified (0–60 dB) complex analog signal is digitized by the USRP motherboard at a fixed rate and resolution (64 MS/s, 12 bit). Due to the bandwidth limitation on the USB bus and the coarse-grained tuning steps of the analog mixer, the FPGA in the digital frontend implements a digital downconversion step before sending the samples to the PC. In the current application, the USB stream is a 1 MS/s complex signal (1 MHz IF bandwidth), and the carriers are around 100 kHz with a few hundred Hz separation. In the IF stage the chirp signal sweeps from DC to 10 kHz.

The lower part of Figure 5 describes the signal processing steps on the software side. On the GNU Radio platform, the signal processing blocks are implemented in C++, but the blocks are configured and wired by Python scripts, which provides a very flexible environment without compromising on performance. Although many of the signal processing steps of the proposed approach (envelope decoding, time synchronization, and filtering) are implemented on the GNU Radio platform, the published results are based on recorded data and offline processing in MATLAB [23]. However, the final signal processing chain contains no steps which are infeasible to implement in a real-time GNU Radio application.

The time synchronization decoder processes the received samples independently from the rest of the signal processing path and produces time reference points at the end of the chain. It uses a matched filter and a peak detector to find the exact position of the chirp signal in the data stream. The current implementation provides 1 microsecond accuracy which is far better than required.

Figure 6 shows the results at key intermediate steps along the main signal processing path. These signals were captured in a stationary setup (both transmitters—one SDR node and one XSM mote [22]—were fixed) to measure the accuracy and repeatability of the proposed approach. At the first stage of the chain, the complex samples are used to calculate the instantaneous signal energy (squared envelope signal). This signal (second in Figure 6) is very noisy and usually has a significant DC component. Also, it has noncomplex samples but a higher than necessary sampling frequency. Thus, before filtering, it goes through a complex digital downconversion step. The next step is essential: it employs a very narrow bandpass filter to remove most of the noise, the DC component, and the images introduced by the digital mixer. The bandpass filter (6th order elliptic IIR) is run-time tuned by a coarse grained FFT-based frequency estimator. The final result of the frequency estimator (real part) is shown on the third line of Figure 6. Note, the frequency of this signal significantly differs from the original envelope frequency due to the digital downconversion step. Since we are interested only in the frequency fluctuation of the signal, this constant shift is irrelevant for ranging purposes. However, the frequency of the digital mixer has to be selected carefully since the unfiltered signal contains many frequency components that might get converted or aliased to near the envelope frequency. Currently, the DDC uses 3/5 of the envelope frequency estimated by the FFT. The complex pairs are processed by a simple FM demodulator which quickly provides an estimate of the instantaneous frequency. Finally, the frequency output is low-pass filtered and decimated.
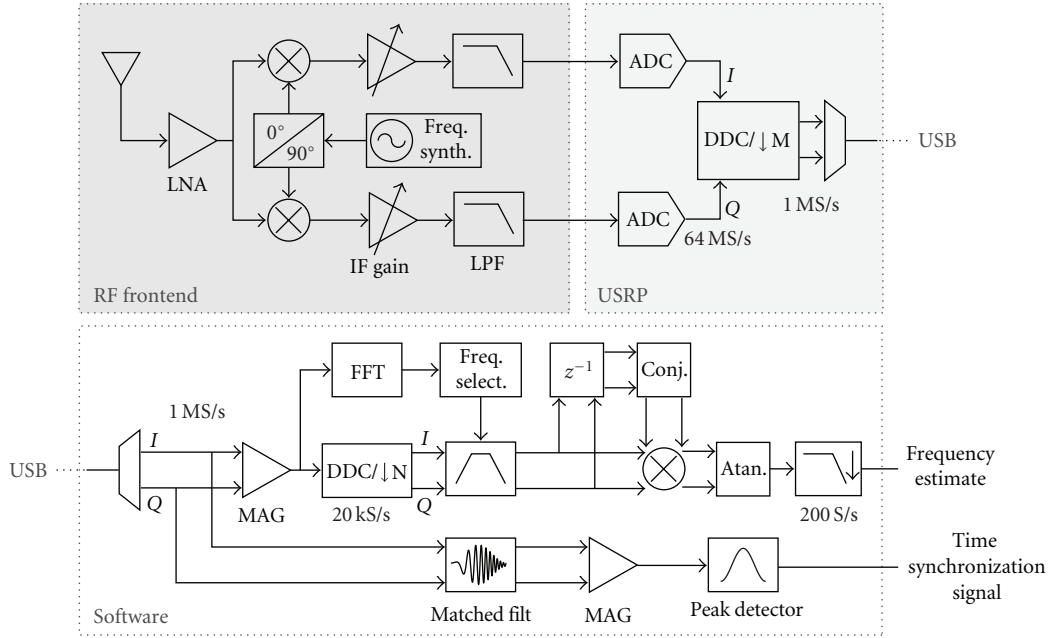
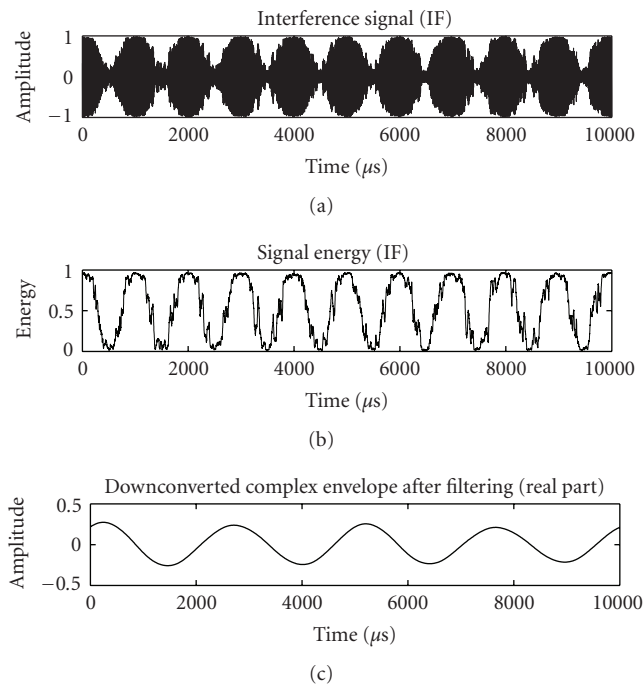FIGURE 5: Signal flow diagram of the receiver node.

(a)

(b)

(c)

FIGURE 6: Captured and processed interference signal.

FIGURE 7: Localization with 3 receivers.

4. Localization

We have shown how to estimate the angle of two RF receivers at known locations from a rotating RF transmitter located at an unknown position. This measurement constrains the node's unknown location to a circle as shown in Figure 3.
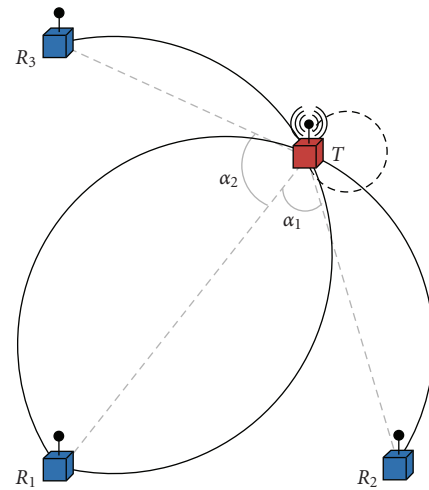
Therefore, to localize the transmitter, an additional measurement is needed. It can be achieved by introducing a third receiver as shown in Figure 7.

Performing the angle estimation for each pair of receivers from the set of R_1, R_2, and R_3, three distinct angles will be obtained ($\alpha_1 : \angle R_1 T R_2$, $\alpha_2 : \angle R_1 T R_3$, $\alpha_3 : \angle R_3 T R_2$). Each angle and the known positions of its corresponding receivers define a circle. Calculating the center of this circle and its radius for each estimate is straightforward and necessary for the localization estimate; however, this task is complicated by the symmetrical properties of the geometry. Each angle and its receivers define not one but two circles that are symmetrical about the chord between the positions of the receivers, that is, the centers of the circles

are reflections about a line connecting the locations of the two receivers. Resolving this dual solution would be impossible without knowing the direction of rotation of the transmitter T. While omitting details, we indicate here that assuming a known direction of rotation, the proper circle can be selected from the angular separation in time of the observed Doppler shifted frequencies between two receivers and their spatial relationship with the calculated centers of the symmetrical circles of interest. More plainly, each solution (circle), provided the assumed direction of rotation, will influence the order in which the two receivers observe their maximum/minimum Doppler shifted frequencies (e.g., either R_1 before R_2 or vice versa).

Accordingly, three unique circles are obtained (one for each α), and the desired localization estimate is calculated from their intersection points. Note that we obtain not one intersection point but up to three, because the circle of rotation is not zero and there is measurement error. Therefore, the localization estimate is formulated as the geometric mean (centroid) of these points.

5. Results

In this section, we present experimental results and characterize the corresponding measurement noise. Then, we provide a simulator that, for a given experiment configuration (coordinates of transmitters and receivers, transmit and sampling frequencies, etc.), generates ideal measurement values, that is, a time series of frequency measurements at each receiver. The location solver's sensitivity to measurement errors is evaluated by feeding in this data perturbed by noise with empirically derived characteristics.

5.1. Experimental Results. Figure 8 shows the frequency estimation results using a stationary setup: one XSM transmitter, one SDR transmitter, and two SDR receivers. Since none of the transmitters is moving, the frequency plots should show a straight horizontal line. However, the results clearly indicate a significant change (3 Hz) in the envelope frequency even during this short-time interval (700 millisecond). This drift is due to the instability of the transmitters' oscillators, and it is measured by the two independent receivers consistently. The right side of Figure 8 gives a clearer picture of the accuracy of the frequency estimation method by showing the difference between the two frequency plots. Ideally, the difference should be zero in this stationary setup. In this particular experiment, it fluctuates between ± 0.1 Hz. In case of a rotating transmitter, the bandwidth of the signal is determined by the speed and radius of rotation. It is typically a few Hz; hence, the output of the frequency estimator could be smoothed by a low-pass filter to increase the SNR.

In a slightly modified configuration, we used two fixed position SDR transmitters and two SDR receivers indoors and executed 300 experiments—one every 10 seconds—as previously described. A single experiment resulted in 100 frequency estimates. During the full set of experiments (50 minutes, 300 000 estimates), the largest difference of the measured envelope frequency was 63.8 Hz, again due to

the instability of the transmit frequency. However, the two receivers never differed by more than 0.5 Hz (maximum error) and the standard deviation of their difference was 0.045 Hz.

The central component of the signal processing chain is the frequency estimator for which many different methods have been developed and published [12, 24, 25]. We selected, implemented, and evaluated some of these, but one of the potential future directions is a more exhaustive study and analysis of the applicability of existing methods.

5.2. Simulator. Currently, the localization estimates are calculated in MATLAB [23] for a given experimental configuration and input data set of frequency measurements. The experimental configuration minimally requires that the positions of at least three static receivers be specified along with the center of rotation of the rotating transmitter T. The known position of the static transmitter T' is provided but does not influence the results. During initialization, the various experimental parameters (e.g., 2D locations of transmit/receive nodes, transmission frequencies, sampling rate, radius of rotation of transmitter T, etc.) are specified. Localization estimates are formulated from either experimental measurements obtained from hardware or generated data. Either form of data consists of the measured Doppler shifted envelope frequencies at each receiver over a time interval. Generated data is calculated from the known geometry of the nodes and the configuration parameters, and the simulator further allows the experimenter to include noise in the generated signals (zero-mean Gaussian noise with adjustable standard deviation).

Each localization estimate from the simulator is formulated according to the steps detailed in Section 2. From an input data set of Doppler shifted frequency measurements, the velocity differences between each pairwise combination of receivers are used to calculate the α angles according to the relationship in (15) and (16). From each calculated α, the corresponding circles are calculated (see Figure 4), and the centroid of their pairwise intersection points forms the localization estimate. The following section will detail preliminary results obtained using our approach and the simulator for estimating the 2D location of a rotating transmitter.

5.3. Simulation Results. For our initial experimental evaluation, we assume three static receivers R_1, R_2, and R_3 positioned on the Cartesian xy-coordinate plane (with axial units in meters) at locations (6, 16), (14, 13), and (7.5, 6), respectively. The input sampling rate of each receiver is 500 Hz. The fixed transmission frequencies of the two transmitters T' and T are 430 MHz and 431 MHz ($\delta f = 1$ kHz), respectively. Regarding the rotating transmitter T, the radius of rotation is 0.12 m, the rate of rotation is 45 RPM ($\omega = 4.71$ rad/s), and the direction of rotation is given to be counterclockwise. Assuming the speed of light is 3.0×10^8 m/s, using (3) and the relationship $-r\omega < v = r\omega$ yields an expected Doppler shift ranging between ± 0.81 Hz at any receiver.
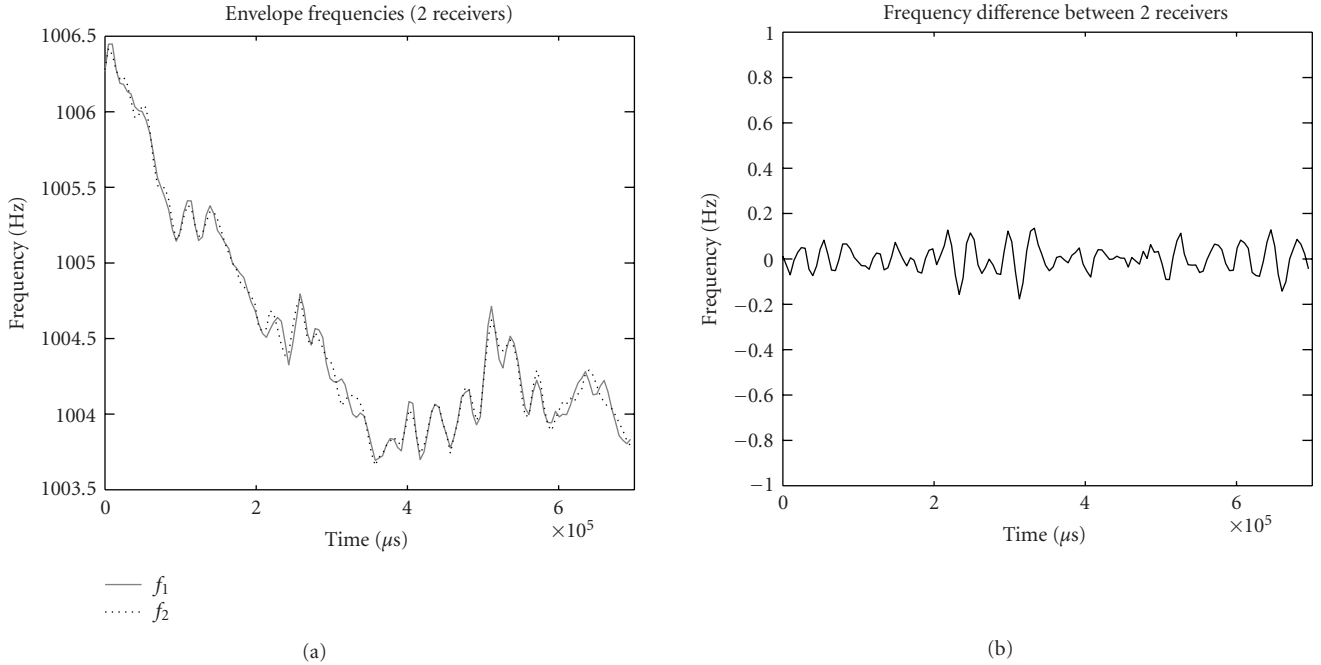
(a)

(b)

FIGURE 8: Frequency estimation results.

With this configuration, we would like to evaluate how accurately we can estimate the center of rotation of T from the calculated α angles using our proposed method. Since the geometry of where T is with respect to the receivers will influence the magnitudes of the α angles, our experimental evaluation needs to generate localization estimates over a range of positions for T that adequately characterizes the field of the receivers. Accordingly, the experimental simulations were conducted by sweeping the location of T from 1 to 21 meters along the x-axis and from 21 to 1 meters along the y-axis in 0.2 m increments (a total of 10,201 unique locations). Simulation results for locations where any receiver is coincident or within the circle of rotation of the rotating transmitter T are ignored. For such a large number of experiments, generated input data was used for the simulations instead of physically-gathered data.

Figure 9 shows the simulation results for the experiment with no noise present in the generated input data. Figure 9(a) is an error plot of the localization estimate over all of the simulated positions of transmitter T. The calculated error is the magnitude of the distance between the known position of T and the estimated position. The colorbar on the right-hand side of the plot shows the color distribution over a range of errors where the units are in meters (localization errors below 0.1 m are white and above 1.0 m are black). The maximum obtained error was 5.5 m which occurred when T was at location $(5.8, 16.2)$, that is, directly adjacent to R_1. We see from Figure 9(a) that almost all significant points of error occur when T lies directly on the lines connecting any two receivers and on the circle defined by the locations of the three receivers. This is intuitive since the former implies at least one calculated α angle that is very near π radians. Such an angle measure results in a very large circle defined

by the method of Figure 4, which is very susceptible to errors. The latter errors are present since the calculated circles from Figure 4 will overlap, that is, a lack of distinct intersection points invalidates the centroid calculation.

Figure 9(b) shows the same type of error plot for the calculated angle α_1 (α angle between receivers R_1 and R_2). The colorbar (in units of radians) indicates calculated α_1's with errors below 0.01 radians are white and above 0.2 radians are black. From the plot we see that the only significant errors occur when T is positioned on the line connecting receivers R_1 and R_2. The presence of the errors can be attributed to two sources: the finite resolution of the calculations for generating the simulation input data and determining the α's and the assumption that the α's are constant while the transmitter is rotating. For the former, as the sampling rate of the receivers is increased, some of the errors decrease to near zero. The latter source of error follows from our approximation that the radius of rotation is negligible compared to the distance between the transmitter and the receivers, and it cannot be generally compensated for or disregarded.

With the frequency estimation results in mind, the same experiment was conducted with zero-mean Gaussian noise added to the generated frequency measurement signals of each of the receivers. The standard deviation of the added noise was set to 6.0% of the maximum expected Doppler shift. This is in line with the error characteristics of the experimentally gathered data. Figure 10 shows the simulation results for this experiment. Notice that the colorbar of Figure 10(a) has been adjusted to have a new upper limit of 3.0 m in order to show the error distribution. The maximum obtained error was 11.69 m which occurred when T was at location $(21, 12)$. We see from Figure 10(a)
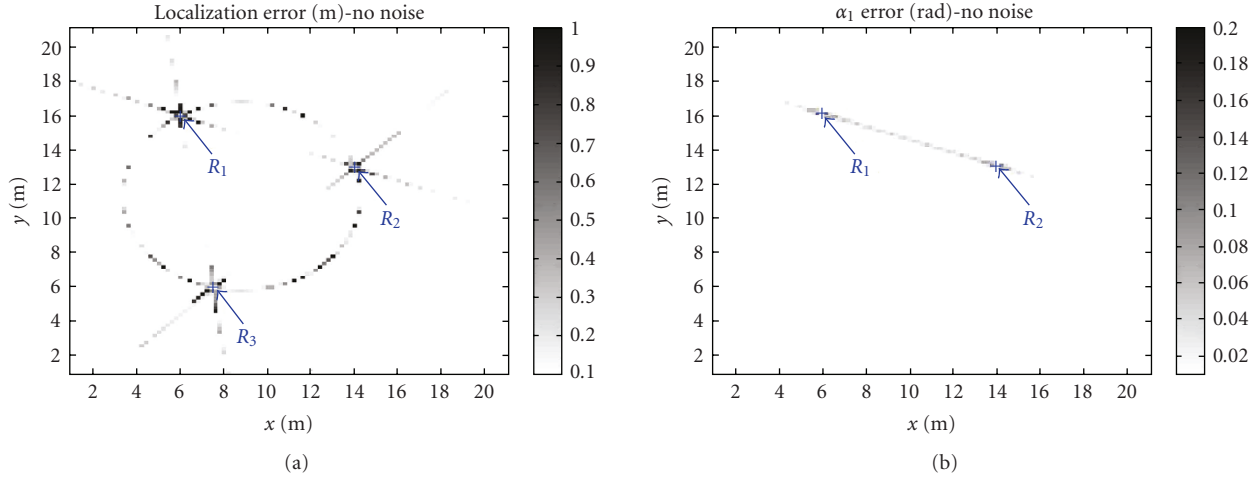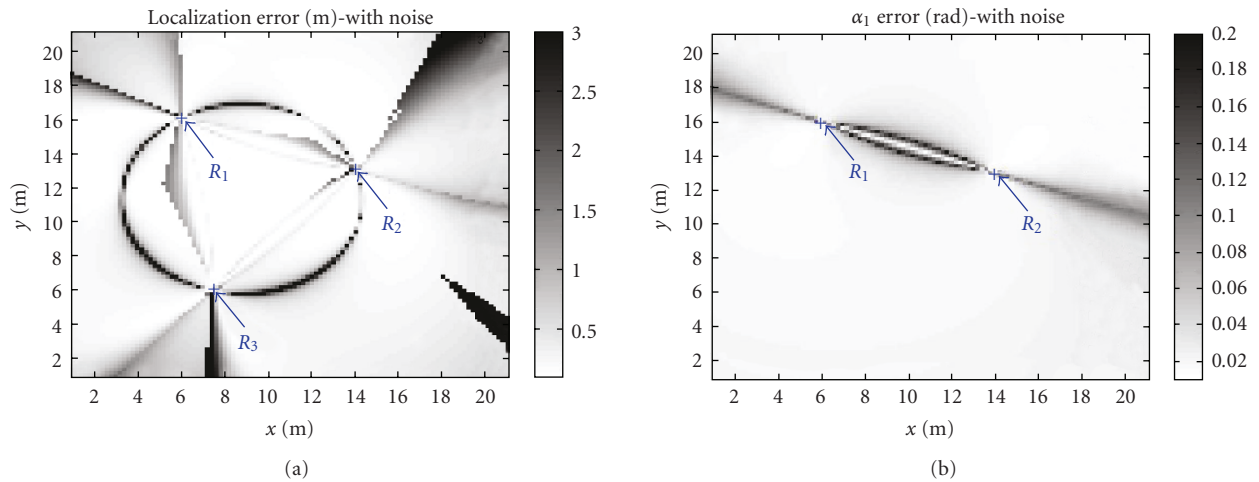
Figure 9: Simulation results with no noise.

Figure 10: Simulation results with noise.

that the majority of the significant errors still occur when T lies directly on the lines connecting any two receivers and on the circle defined by the locations of the three receivers; however, as expected, a larger distribution of errors is present with gradual degradations in accuracy where the degenerate geometries exist. Note that inside the triangle formed by the three receivers, other than close to the edges of the triangle, the error is uniformly below 0.1 m. As can be seen in the figure, significant areas outside the triangle have low error also. Adding a fourth receiver could eliminate the "blind spots" of our method by placing them in such a way that any point can be localized accurately using three out of the four receivers. However, we leave this to future work.

Figure 10(b) shows the error plot for the calculated angle α_1 with the noisy input data. The colorbar distribution is the same as the previous experiment (α_1's with errors below 0.01 radians are white and above 0.2 radians are black). We observe the errors along the line connecting the receivers are accentuated. Note the interesting error pattern along the line in between the receivers; the largest errors along the

line occur at a distance of about one radius (r of T) off the line. This phenomenon can most likely be attributed to the influence of the noise on the α calculations in conjunction with the zero-radius approximation inherent in our method.

6. Conclusion

We presented a novel idea for ranging and localization of wireless radio nodes and our preliminary work validating it. While we have not carried out measurements with an actual rotating transmitter, the stationery experiments and simulation results indicate that the method is not only feasible, but has the potential for achieving high-accuracy localization. In fact, we have barely scratched the surface of what's possible. We have not explored different cases, for example, where the rotating transmitter is at a known position and the tracked node is a receiver. We have not assumed that the rotating node can be synchronized to the receivers, which could provide bearing information. If

the transmit frequency is stabile in the short term (using, e.g., an oven-controlled oscillator), then measuring the maximum of the Doppler shift provides 3D bearing since the maximum observable speed in the plane of the rotation is given by the known radius and angular rate. However, our next logical step needs to be the construction of a stabile rotating platform and a large-scale experiment to validate the method under real-world conditions.

One might question the practical applicability of a rotating node (or antenna). Obviously, in most tracking applications the tags need to be small and inexpensive, so rotation is not really an option. However, in many applications the coverage area is fixed and can be equipped with more expensive, so-called infrastructure nodes. For example, one can imagine a large stadium being equipped with a few rotating nodes at known locations forming the anchor nodes of the system. In a mobile application, a few vehicles can have both GPS for tracking their own positions and the rotating nodes for tracking possibly many other nodes that do not have GPS. Finally, a smart antenna array may be able to mimic the rotation of the transmitter, thus making the system cheaper, more robust and energy efficient.

Acknowledgment

References

[1] P. Bahl and V. N. Padmanabhan, "RADAR: an in-building RF-based user location and tracking system," in *Proceedings of the 19th Annual Joint Conference of the IEEE Computer and Communications Societies (INFOCOM '00)*, vol. 2, pp. 775–784, Tel Aviv, Israel, March 2000.

[2] M. Youssef and A. Agrawala, "The Horus WLAN location determination system," in *Proceedings of the 3rd International Conference on Mobile Systems, Applications, and Services (MobiSys '05)*, pp. 205–218, Seattle, Wash, USA, June 2005.

[3] K. Whitehouse, *The design of Calamari: an ad-hoc localization system for sensor networks*, M.S. thesis, University of California at Berkeley, Berkeley, Calif, USA, 2002.

[4] PinPoint, RFTechnologies, 2008, http://www.ilevel.net/rft/pinpoint/index.htm.

[5] D. Taubenheim, S. Kyperountas, and N. Correal, "Distributed radiolocation hardware core for IEEE 802.15.4," Tech. Rep., Motorola Labs, Plantation, Fla, USA, 2005.

[6] L. M. Ni, Y. Liu, Y. C. Lau, and A. P. Patil, "Landmarc: indoor location sensing using active RFID," in *Proceedings of the 1st IEEE International Conference on Pervasive Computing and Communications (PerCom '03)*, pp. 407–415, Fort Worth, Tex, USA, March 2003.

[7] Pango, 2008, http://www.pangonetworks.com.

[8] N. S. Correal, S. Kyperountas, Q. Shi, and M. Welborn, "An UWB relative location system," in *Proceedings of IEEE Conference on Ultra Wideband Systems and Technologies (UWBST '03)*, pp. 394–397, Reston, Va, USA, November 2003.

[9] Ubisense, 2008, http://www.ubisense.net.

[10] D. P. Young, C. M. Keller, D. W. Bliss, and K. W. Forsythe, "Ultra-wideband (UWB) transmitter location using time difference of arrival (TDOA) techniques," in *Proceedings of the 37th Asilomar Conference on Signals, Systems and Computers (ACSSC '03)*, vol. 2, pp. 1225–1229, Pacific Grove, Calif, USA, November 2003.

[11] R. J. Fontana, E. Richley, and J. Barney, "Commercialization of an ultra wideband precision asset location system," in *Proceedings of IEEE Conference on Ultra Wideband Systems and Technologies (UWBST '03)*, pp. 369–373, Reston, Va, USA, November 2003.

[12] M. Maróti, B. Kusý, G. Balogh, et al., "Radio interferometric geolocation," in *Proceedings of the 3rd ACM Conference on Embedded Network Sensor Systems (SenSys '05)*, pp. 1–12, San Diego, Calif, USA, November 2005.

[13] B. Kusý, Á. Lédeczi, M. Maróti, and L. Meertens, "Node density independent localization," in *Proceedings of the 5th International Conference on Information Processing in Sensor Networks (IPSN '06)*, pp. 441–448, Nashville, Tenn, USA, April 2006.

[14] B. Kusý, G. Balogh, J. Sallai, Á. Lédeczi, and M. Maróti, "inTrack: high precision tracking of mobile sensor nodes," in *Proceedings of the 4th European Workshop on Wireless Sensor Networks (EWSN '07)*, pp. 51–66, Delft, The Netherlands, January 2007.

[15] B. Kusý, J. Sallai, G. Balogh, et al., "Radio interferometric tracking of mobile wireless nodes," in *Proceedings of the 5th International Conference on Mobile Systems, Applications and Services (MobiSys '07)*, pp. 139–151, San Juan, Puerto Rico, USA, June 2007.

[16] A. Harter, A. Hopper, P. Steggles, A. Ward, and P. Webster, "The anatomy of a context-aware application," in *Proceedings of the 5th ACM/IEEE International Conference on Mobile Computing and Networking (MobiCom '99)*, pp. 59–68, Seattle, Wash, USA, August 1999.

[17] R. Want, A. Hopper, V. Falcão, and J. Gibbons, "The active badge location system," *ACM Transactions on Information Systems*, vol. 10, no. 1, pp. 91–102, 1992.

[18] A. S. Chipcon, "CC1000: single chip very low power RF transceiver," 2004, http://www.chipcon.com.

[19] B. Kusý, Á. Lédeczi, and X. Koutsoukos, "Tracking mobile nodes using RF doppler shifts," in *Proceedings of the 5th ACM Conference on Embedded Network Sensor Systems (SenSys '07)*, pp. 29–42, Sydney, Australia, November 2007.

[20] GNU Radio, 2008, http://gnuradio.org/trac.

[21] Ettus Research LLC, 2008, http://www.ettus.com.

[22] P. Dutta, M. Grimmer, A. Arora, S. Bibyk, and D. Culler, "Design of a wireless sensor network platform for detecting rare, random, and ephemeral events," in *Proceedings of the 4th International Conference on Information Processing in Sensor Networks (IPSN '05)*, pp. 497–502, Los Angeles, Calif, USA, April 2005.

[23] Mathworks Simulink/Stateflow Tools, 2008, http://www.mathworks.com.

[24] M. R. Petraglia, S. K. Mitra, and J. Szczupak, "Adaptive sinusoid detection using IIR notch filters and multirate techniques," *IEEE Transactions on Circuits and Systems II*, vol. 41, no. 11, pp. 709–717, 1994.

[25] B. G. Quinn and E. J. Hannan, *The Estimation and Tracking of Frequency*, Cambridge University Press, Cambridge, UK, 2001.